

Strong tangential force within a small trapping volume under near-field Laguerre-Gaussian beam illumination

Baohua Jia*, Xiaosong Gan, and Min Gu

Center for Micro-Photonics, Faculty of Engineering and Industrial Sciences,
Swinburne University of Technology, P.O. Box 218 Hawthorn, 3122 Australia

*Corresponding author: bjia@swin.edu.au

Abstract: Near-field rotation of a trapped particle under focused evanescent Laguerre-Gaussian beam illumination is theoretically investigated by mapping the two-dimensional transverse trapping efficiency exerting on the particle. It is revealed that the severe focal field deformation associated with a focused evanescent Laguerre-Gaussian beam causes a significant impact on the transverse trapping performance of the microparticle. Compared with the far-field trapping force, strong tangential force components have been observed in the transverse efficiency mapping, which potentially lead to rotational motions to the particle within a small trapping volume in the optical near-field.

©2008 Optical Society of America

OCIS codes: (260.1960) Diffraction theory; (140.7010) Laser trapping; (110.0180) Microscopy.

References and links

1. A. Ashkin, "Forces of a single-beam gradient laser trap on a dielectric sphere in the ray optics regime," *Biophys. J.* **61**, 569-582 (1992).
2. J. P. Barton, D. R. Alexander, and S. A. Schaub, "Theoretical determination of net radiation force and torque for a spherical particle illuminated by a focused laser beam," *J. Appl. Phys.* **66**, 4594-4602 (1989).
3. D. Ganic, X. Gan, and M. Gu, "Trapping force and optical lifting under focused evanescent wave illumination," *Opt. Express* **12**, 5533-5538 (2004).
4. A. T. O'Neil and M. J. Padgett, "Three-dimensional optical confinement of micron-sized metal particles and the decoupling of the spin and orbital angular momentum within an optical spanner," *Opt. Commun.* **185**, 139-143 (2000).
5. H. Rubinsztein-Dunlop, T. A. Nieminen, M. E. J. Friese, and N. R. Heckenberg, "Optical trapping of absorbing particles," *Adv. Quantum Chem.* **30**, 469-492 (1998).
6. M. Gu, J.-B. Haumonte, J. Chon, and X. Gan, "Laser trapping and manipulation under focused evanescent wave illumination," *Appl. Phys. Lett.* **84**, 4236-4238 (2004).
7. R. F. Marchington, M. Mazilu, S. Kuriakose, V. Garcés-Chávez, P. J. Reece, T. F. Krauss, M. Gu, and K. Dholakia, "Optical deflection and sorting of microparticles in a near-field optical geometry," *Opt. Express* **16**, 3712-3726 (2008).
8. S. Kuriakose, D. Morrish, X. Gan, J.W.M. Chon, K. Dholakia, M. Gu, "Near-field optical trapping with an ultrashort pulsed laser beam," *Appl. Phys. Lett.* **92**, 081108 (2008).
9. M. Gu, S. Kuriakose, and X. Gan, "A single beam near-field laser trap for optical stretching, folding and rotation of erythrocytes," *Opt. Express* **15**, 1369-1375 (2007).
10. M. Gu, *Advanced Optical Imaging Theory* (Springer, Heidelberg, 2000).
11. B. Jia, X. Gan, and Min Gu, "Direct observation of pure focused evanescent wave of a high numerical aperture objective lens by scanning near-field optical microscopy," *Appl. Phys. Lett.* **86**, 131110 (2005).
12. L. Novotny, R. X. Bian, and X. S. Xie, "Theory of nanometric optical tweezers," *Phys. Rev. Lett.* **79**, 645-648 (1997).
13. K. Okamoto and S. Kawata, "Radiation force exerted on subwavelength particles near a nanoaperture," *Phys. Rev. Lett.* **83**, 4534-4537 (1999).
14. L. Allen, M. W. Beijersbergen, R. J. C. Spreeuw, and J. P. Woerdman, "Orbital angular-momentum of light and transformation of Laguerre-Gaussian laser modes," *Phys. Rev. A* **45**, 8185-8189 (1992).
15. D. G. Grier, "A revolution in optical manipulation," *Nature* **424**, 810-816 (2003).
16. W. M. Lee, X.-C. Yuan, and W. C. Cheong, "Optical vortex beam shaping by use of highly efficient irregular spiral phase for optical micromanipulation," *Opt. Lett.* **29**, 1796-1798 (2004).

17. B. Jia, X. Gan, and M. Gu, "Anomalous phenomenon of a focused evanescent Laguerre-Gaussian beam," *Opt. Express* **13**, 10360-10366 (2005).
 18. D. Ganic, X. Gan, and M. Gu, "Exact radiation trapping force calculation based on vectorial diffraction theory," *Opt. Express* **12**, 2670-2675 (2004).
 19. T. Funatsu, Y. Harada, M. Tokunaga, K. Saito and T. Yanagida, "Imaging of single fluorescent molecules and individual ATP turnovers by single myosin molecules in aqueous solution," *Nature* **374**, 555-559 (1995).
-

1. Introduction

Optical tweezers have been widely used in the fields of modern physics, chemistry and biology for confinement and manipulation of microparticles, biological cells and molecules [1-5]. Recently near-field trapping using a focused evanescent field generated by a high numerical aperture (NA) total internal reflection (TIR) objective illuminated with an annular beam has been demonstrated to be advantageous over the far-field trapping scheme in biological samples [6-9], and in particular the red blood cells [9]. This is due to a significantly reduced focal volume, which can substantially suppress the background and the heating effect [3, 6-11]. In the mean time, rotation mechanisms, which are of great importance to achieve a complete manipulation of the trapped microobjects, can be potentially introduced by dynamically controlling the phase, amplitude or even the polarization states of the incident beam. However, for other near-field trapping methods [12,13], for example using a fiber tip, rotation is rather difficult to achieve.

Laguerre-Gaussian (LG) beams, which carry orbital angular momentum by their helical phase front, are commonly utilized in far-field trapping to achieve a completely controllable manipulation of the trapped object [14-16]. The electric field of such a beam can be expressed as $E = E_0 \exp(im\varphi)$, where φ is the polar coordinate in the plane perpendicular to the beam axis and m is called the topological charge. It has been revealed recently that when the LG beams are combined with the focused evanescent field, an anomalous focal field deformation occurs due to the phase dislocation induced by TIR and the helical phase front of the LG beams [17]. Spiral intensity patterns with the shapes similar to the optical spanner [15] were observed in the focal region of the objective. Such an asymmetric focal field is favorable for generating a controllable rotation of a homogeneous sphere in the near-field region by only utilizing single LG beam illumination. In this paper, the near-field trapping force on a microparticle under a focused evanescent LG beam illumination is investigated theoretically. The rotational motion is examined by mapping the two-dimensional (2D) transverse force exerting on a polystyrene particle.

2. Deformation of a focused evanescent field under LG beam illumination

LG beams are known for their characteristic intensity distributions of a dark spot on the optical axis surrounded by a bright ring. However when focused by a high NA objective, they lose their radial symmetry and two distinctive intensity maxima appear perpendicular to the incident polarization direction due to the presence of a significant longitudinal polarization component [3, 10, 11]. The deformation of the focal field becomes more pronounced when the TIR condition is met. Using the vectorial Debye theory [10] the intensity distributions of the focal field and their components ($|E_x|^2$, $|E_y|^2$, and $|E_z|^2$) under horizontally polarized LG beam ($m=0-3$) illumination are calculated and depicted in Fig. 1. To produce a pure focused evanescent field at a cover glass ($n_1=1.78$) and air ($n_2=1$) interface, an obstruction disk with a normalized radius $\rho = 0.8$ is inserted at the back aperture of a high NA objective ($NA = 1.65$) to block all the propagating components. Influenced by the phase shift induced by the TIR, prominent changes occur to all the field components [17]. Compared with the field components of a Gaussian beam (Figs. 1(a)-1(c)), all the three polarization components and the overall fields of the focused evanescent LG beams lose their symmetries (Figs. 1(d)-1(p)). However, due to the dominant strengths of the $|E_x|^2$ and $|E_z|^2$ components, which are one order of magnitude stronger than the $|E_y|^2$ component, the overall distributions of the foci exhibit spanner shapes (Figs. 1(h), 1(l) and 1(p)).

Since the rotation of the focal fields are directly caused by the TIR, the rotation angle (α) of the field, which can be defined as the angle between the intensity maxima with respect to the vertical direction, as shown in Fig. 2(a), has a strong dependence on the obstruction size. In Fig. 2(b), the rotation angle α is plotted as a function of the normalized obstruction radius for different topological charges ($m=0-4$). For non-zero charges the rotation angle first decreases steadily as the obstruction radius becomes large and reaches the minimum value at the critical radius ρ_c (corresponding to the critical angle). When the focused field becomes purely evanescent, i.e. $\rho > \rho_c$, the rotation angle α increases steeply and monotonically with increasing the obstruction radius. It is important to note that the focus rotation persists as long as there is an evanescent component, which suggests that it is an intrinsic phenomenon of any objective operating under the TIR condition. Another noticeable feature in Fig. 2(b) is that the rotation angle varies as a function of the topological charge. For the same obstruction size, the rotation angle is larger for lower topological charges. This feature allows another freedom to control the field rotation by applying LG beams of different topological charges.

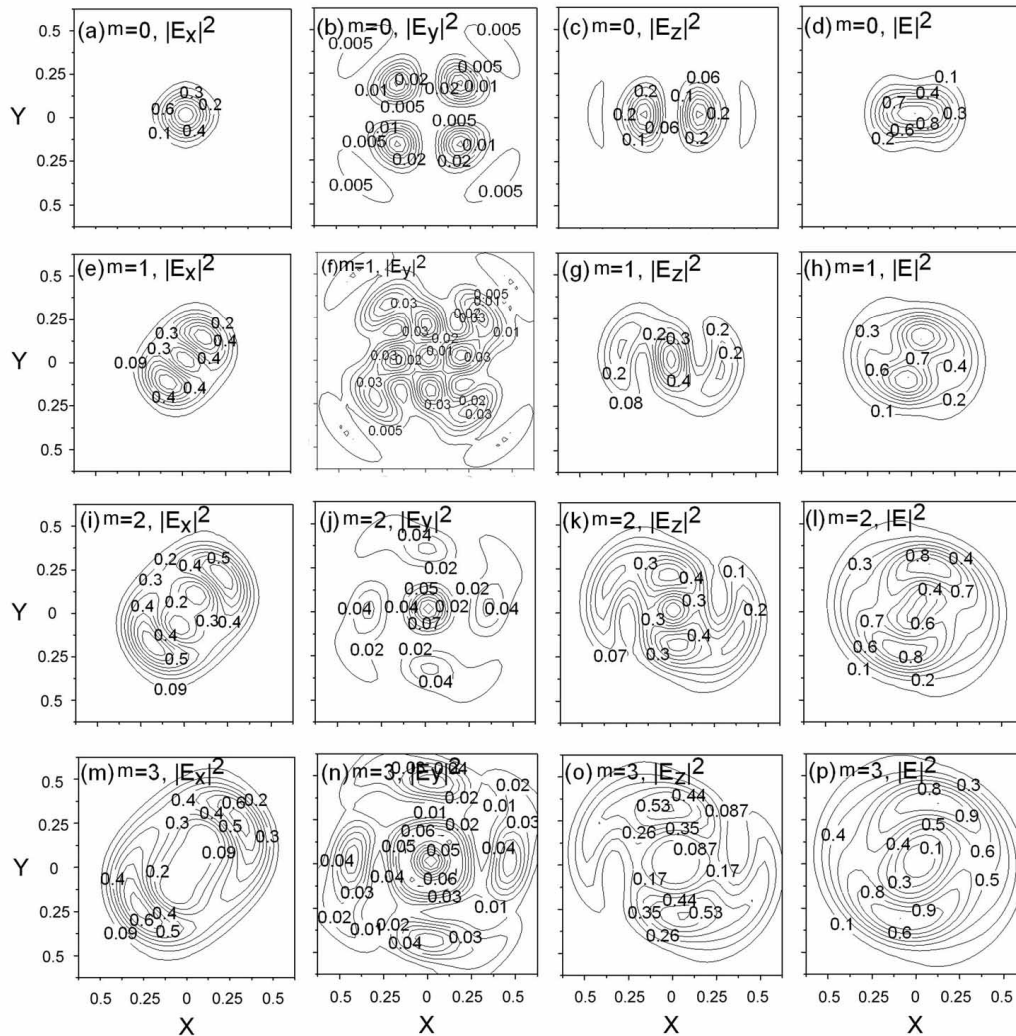


Fig. 1. Normalized intensity distributions ($|E|^2$) and their field components ($|E_x|^2$, $|E_y|^2$, and $|E_z|^2$) in the focal region of an objective with NA = 1.65 at the coverglass ($n_1 = 1.78$) and air ($n_2 = 1$) interface, illuminated by annular ($\rho=0.8$) LG beams of topological charges 0-3. Light polarization in x direction. Unit of axes: μm .

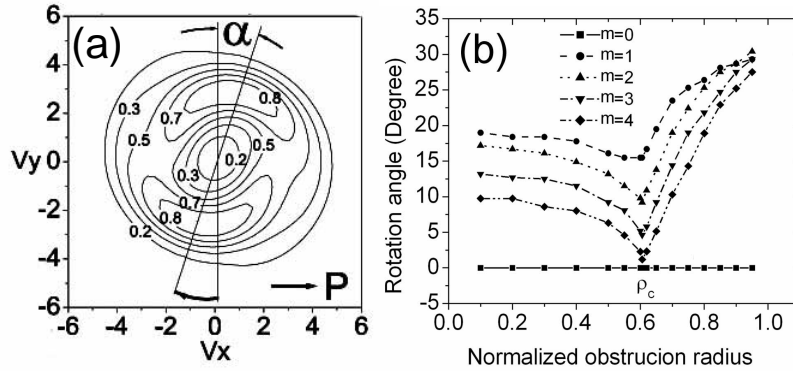


Fig. 2. (a). Definition of a rotation angle α . $V_x=k_x \sin\phi$, $V_y=k_y \sin\phi$. (b) Rotation angle as a function of the normalized obstruction radius for topological charges 0 to 4 ($NA = 1.65$, $n_1 = 1.78$, $n_2 = 1$).

3. Transverse force mapping

The severely distorted spanner shaped focal field could possibly result in rotational motion to a trapped particle in the near-field region. To evaluate the rotational motion of a polystyrene particle trapped under a focused evanescent LG beam, 2D transverse trapping force has been calculated. Similar calculation was conducted previously using a model based on the combination of the vectorial diffraction theory and the Maxwell stress tensor approach [18]. However due to the assumption of a symmetric focal field distribution of LG beams, it was only performed on two orthogonal axes [3]. Because of the severe asymmetrical focal field distributions of the focused evanescent LG beams [17], it is indeed essential to undertake a complete 2D mapping of the transverse trapping force.

Considering a monochromatic electric magnetic (EM) field enters from the first medium (n_1) to the second medium (n_2) to illuminate a homogeneous microsphere situated in the second medium, the net radiation force on the microsphere can be expressed as [18]

$$\langle F \rangle = \frac{1}{4\pi} \int_0^{2\pi} \int_0^\pi \{ \epsilon_2 E_r \mathbf{E} + H_r \mathbf{H} - \frac{1}{2} (\epsilon_2 E^2 + H^2) \hat{r} \} r^2 \sin\phi d\phi d\theta \quad (1)$$

where r , ϕ and θ are spherical polar coordinates, E_r and H_r are the radial parts of the resulting EM field evaluated on the spherical surface enclosing the particle. A dimensionless parameter trapping efficiency Q , which is independent of the trapping power (P), is used to evaluate the trapping force (F). It is defined as $Q = Fc/nP$, where c is the speed of light in vacuum.

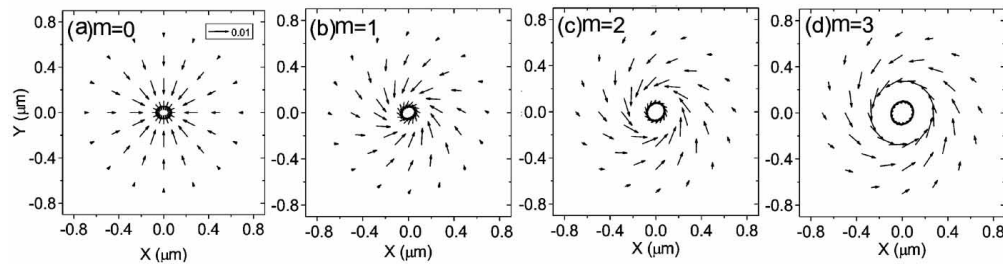


Fig. 3. Transverse trapping efficiency mapping for a polystyrene particle of $1 \mu\text{m}$ in radius across a pure focused evanescent field generated by an objective with $NA = 1.65$ and $\rho = 0.85$, at the coverslip ($n_1 = 1.78$) and water ($n_2 = 1.33$) interface under LG beam illumination ($m = 0, 1, 2$ and 3 , light polarization in x direction).

Figure 3 presents the 2D mapping of the transverse trapping efficiency for a polystyrene particle of $1 \mu\text{m}$ in radius (a) trapped in a pure focused evanescent field ($\lambda=532 \text{ nm}$) generated

by the obstructed TIR objective (NA=1.65, $\rho = 0.85$) at a coverglass ($n_1 = 1.78$) and water ($n_2 = 1.33$) interface under LG beam illumination ($m = 0, 1, 2$ and 3). A stable near-field trapping can be obtained under such a circumstance [3]. As expected, when a plane wave ($m=0$) is utilized in Fig. 3(a), the transverse trapping efficiency is directed towards the center of the focal region because of the gradient force. No evident tangential component appears in the trapping efficiency mapping. However, when non-zero charges are applied (Figs. 3(b)-3(d)), significant tangential force components start to emerge as a result of the asymmetric focal field distributions. Furthermore, the tangential force becomes stronger for higher topological charges due to a larger light-particle interaction area resulted from a larger field distribution. The weighting of the tangential force component increases with the topological charge. When $m=3$ is applied (Fig. 3(d)), it reaches nearly 100% of the total force at $b = 0.3 \mu\text{m}$, where b is the radial coordinate in the 2D plane and defined as $b = \sqrt{x^2 + y^2}$. Such strong tangential force components could result in the near-field trapped microsphere to rotate around the focal center.

Tangential force components can also be observed when a far-field LG beam is employed, however with a much reduced strength. For example, in Fig. 4 the transverse trapping efficiency for the same polystyrene particle across the far-field focal region generated by an objective with NA = 1.2 at the coverslip ($n_1 = 1.51$) and water ($n_2 = 1.33$) interface under LG beam illumination are mapped for 8 topological charges. For $m=0-3$, no obvious tangential components can be observed. The tangential components only become noticeable when the topological charge is larger than 6, as shown in Fig. 4(h). The trapping efficiency mapping has also been performed for other particle sizes and objectives with different NAs under far-field illumination. Similar results (not shown) to those observed in the NA=1.2 objective have been achieved. This indicates that in the case of high angle far-field focusing, higher topological charges are essential for achieving a noticeable tangential force component.

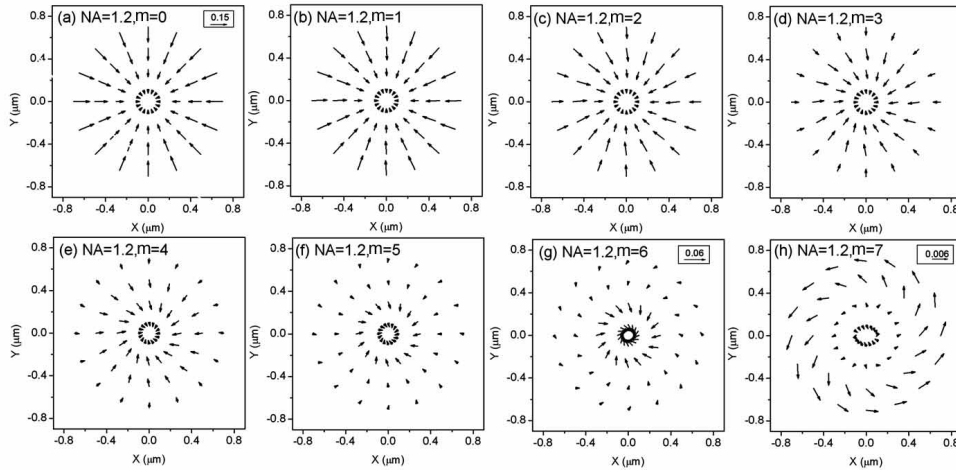


Fig. 4. Transverse trapping efficiency mapping for a polystyrene particle of $1 \mu\text{m}$ in radius across the focal field generated by a NA = 1.2 objective at the coverslip ($n_1 = 1.51$) and water ($n_2 = 1.33$) interface under LG beam illumination ($m = 0-7$, light polarization in x direction). Scale bar in (a) also applies to (b-f).

To demonstrate this point more explicitly, the tangential components for nine different topological charges focused by two objectives (NA=1.65 and NA=1.2) were extracted from the force mapping and compared in Fig. 5 for four positions ($b = 0.1a, 0.3a, 0.5a$ and $0.7a$), respectively. It is clearly seen from Fig. 5(a) that in the case of the obstructed TIR objective (NA=1.65, $\rho=0.85$), for all the four positions, the tangential force components are dominant in the force mapping for higher topological charges ($m>1$). For instance, when a charge of 4 is utilized, the tangential component increases to almost 100% of the entire force vector

implying that a rotational motion is most likely to be introduced under such a circumstance. Even when low topological charge ($m=1$) is employed, the tangential force component still remains approximately 50%. In contrast, in the case of far-field LG beams (Fig. 5(b)), the tangential components are much weaker. In most cases they are less than 50%, except when n is high ($m>6$). Strong tangential components approaching 100% only occur when $m=7$ at a specific position ($b=0.7a$). The dominant tangential force components observed in the near-field trapping scheme can be attributed to the significant impact caused by the spanner shape of the focused evanescent field.

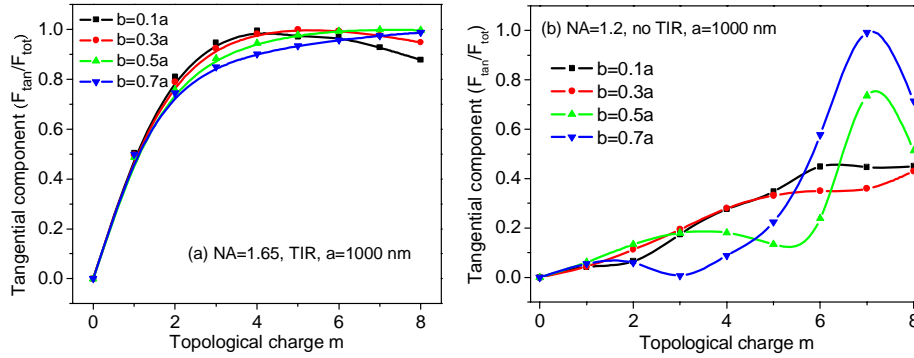


Fig. 5. Dependence of the tangential force components on the topological charges of (a) the focused evanescent LG beams ($NA=1.65$, $\rho = 0.85$) (b) far-field LG beams ($NA=1.2$) at different radial positions ($b = 0.1a, 0.3a, 0.5a$ and $0.7a$).

4. Focal volume and angular momentum comparison

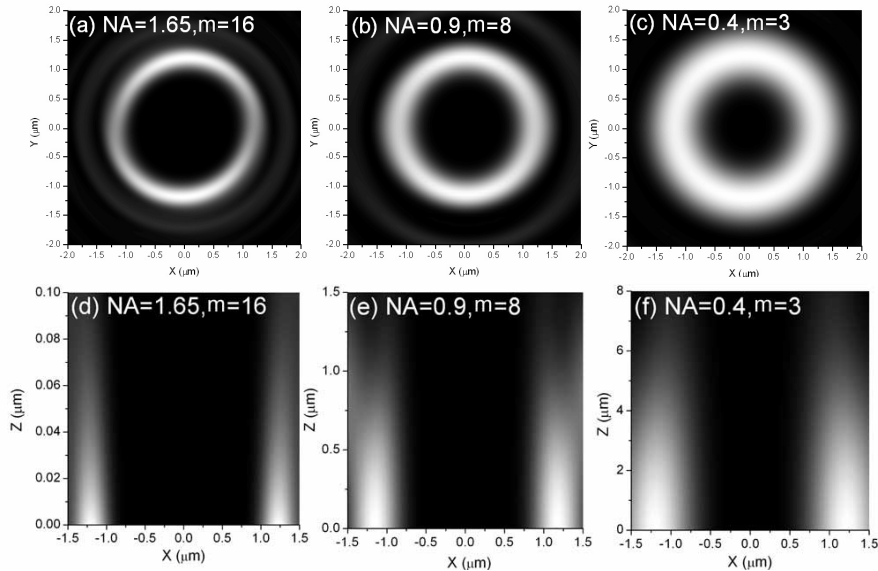


Fig. 6. Focal intensity distributions in (a-c) the focal plane and (d-f) the X-Z plane of (a,d) an evanescent LG beam of $m = 16$, focused by $NA = 1.65$ objective; (b,e) a far-field LG beam of $m = 8$, focused by a $NA=0.9$ objective; (c,f) a far-field LG beam of $m = 3$, focused by a $NA=0.4$ objective.

Focused evanescent LG beams not only show much more dominant tangential force components, but also possess significantly reduced focal volume, which is highly desirable for a variety of nanometric biological samples [6-9,19]. For example, as presented in Figs. 6(a)-

6(c), to generate a similar ring size ($a=1.2\ \mu\text{m}$) to trap a particle, a TIR objective ($\text{NA} = 1.65$) requires a topological charge of $m = 16$, while a high NA far-field objective ($\text{NA}=0.9$) requires $m=8$ and a low NA objective ($\text{NA}=0.4$) requires $m=3$, respectively. Although the transverse ring sizes are similar, the axial sizes of the focal fields exhibit enormous differences due to the different focusing strength of each objective, as presented in Figs. 6(d-f). The focused evanescent LG beam (Fig. 6(d)) is localized closely within the vicinity of the interface. If a focal depth (d) is defined as the distance from the interface to the point where the intensity drops to $1/e$ of its maximum, the focal depth is $0.05\ \mu\text{m}$ in the case of Fig. 6(d). In contrast, the far-field LG beams show much extended focal fields in the axial direction (z axis). Focal depths of $0.85\ \mu\text{m}$ and $4.5\ \mu\text{m}$ have been found for objectives with $\text{NA} = 0.9$ and $\text{NA}=0.4$, respectively, as shown in Figs. 6(e) and 6(f). Based on the ring size and the focal depth of each field, one would find that the focal volume of a focused evanescent LG beam is 90 and 17 times smaller than those of the far-field LG beams focused by the $\text{NA}=0.4$ and $\text{NA} = 0.9$ objectives, respectively.

Advantages of using focused evanescent LG beams in laser trapping are not limited to a significantly reduced focal volume. It is well known that a light beam with an azimuthal phase dependence of $\exp(im\phi)$, like a LG beam, carries an orbital angular momentum with a value of $L = m\hbar$ per photon [14]. This indicates that using a high charged focused evanescent LG beam instead of a low charged far-field LG beam to trap a particle results in much higher orbital angular momentum provided that the similar sized ring patterns are required. As an example, in Fig. 6 in order to generate LG beams of a similar ring size in the cases of (a) and (c), a topological charge of 16 is required in the $\text{NA}=1.65$ objective, instead of $m = 3$ in the $\text{NA}=0.4$ objective, which results in a much higher angular momentum in the near-field scheme.

4. Conclusion

In conclusion, the influence of the asymmetric focal intensity distribution of a focused evanescent LG beam on near-field laser trapping of a homogeneous microparticle is studied. By mapping the transverse trapping efficiency exerting on the particle under the illumination of both far-field and near-field LG beams, it has been revealed that a significantly increased tangential force component can act on the particle under the near-field illumination suggesting that the spanner shaped focal field distribution is the main reason contributing to the tangential component. Under such a circumstance, a controllable rotational motion is potentially to be generated on the trapped homogeneous particle in the optical near-field with a single LG beam. The findings may prove useful for a variety of biological applications, including single molecule detection [6-9,19].

Acknowledgment

The authors acknowledge the Australian Research Council for its support. The authors thank Dr. Djenan Ganic for his useful discussion on this topic.